Fuku, X. et al. (2018). An electrochemically active green synthesized polycrystalline NiO/MgO catalyst: Use in photo-catalytic applications.
Materials Research Bulletin, 97: 457 – 465
http://dx.doi.org/10.1016/j.materresbull.2017.09.022

An electrochemically active green synthesized polycrystalline NiO/MgO catalyst: Use in photo-catalytic applications

X. Fuku, N. Matinise, M. Masikini, K. Kasinathan and Malik Maaza

Abstract

For many years, research scientists have aided communities in their tremendous efforts towards environmental remediation. Due to their high physical and chemical stability, metal oxide nanoparticles (NPs) have been used as metal catalysts to remedy this issue. This article reviews green approaches for the synthesis of metal oxide nanoparticles, in aqueous bio-reductive polyphenols from punica granatum peel extract and the degradation of organic pollutants. The bimetallic nanocomposite of face-centred cubic NiO/MgO pseudocapacitors were successfully prepared via the polyphenols of punica granatum peel extracts. X-ray diffraction spectroscopy (XRD) successfully provide evidence of polycrystalline face-centre cubic nanocomposite (high crystallinity index (I_{cry}) > 1) while revealing their interplanar distance. The spherical and irregular particle distribution of the binary NiO/MgO nanocomposite (at different calcination temperatures) was assessed by high resolution-TEM. FTIR, GC–MS and EDS provided evidence of the proposed mechanism during coordination between polyphenols and metal precursors. The popular "egg box model" is referred to in the case of polyphenols-metal interaction. The unique feature of two consecutive chelation site per repeat that provides a favourable entropic contribution to the inter-chain association is produced by this model governed by electrostatic interactions. Based on the obtained results, new structural models of Ni^{2+}/Mg^{2+}-polyphenols (punicalagin) complexes were proposed. UV–vis and Cyclic voltammetry confirmed the growth and band gap energies of the nanocomposite. NiO/MgO nanocomposite was found to be excellent photocatalysts for the degradation of methylene orange and methylene blue under the illumination of artificial light irradiation. The experiments demonstrated that MB in aqueous solution was more efficiently photo-degraded (87%) than MO (73%) using NiO/MgO nanocomposite as photocatalysts within 10 min of exposure. Conclusively, the nanocomposite was found to be more efficient compared to other reported oxides.

1. Introduction

For the past decade a number of innovate materials in a nano-scale range have been synthesized via a wide range of green, chemical and physical methods. The unique properties of the prepared nanomaterials make them valuable materials hence their wide employement in various fields including photoelectric, catalysts, sensors, solar absorbers, energy, and

many others [1–4]. Metal oxides are one of the nanomaterials which are finding a wide range of applications as catalysts for detection of heavy metals, environmental pathogens, organic and inorganic pollutants since they possess special properties, i.e., high reactivity, high specific surface area, controlled size and distribution [1–4]. Common metal oxides such as MgO, TiO_2, CaO, NiO and ZnO have been shown to be highly efficient and active adsorbents for many toxic chemicals including air pollutants, chemical warfare agents, acidic gases, and water pollution [1,3]. In particular, the high surface reactivity, high chemical and thermal stability makes MgO a promising material for different applications [5,6]. Nanosized MgO is a functional material that has been widely used in various areas and recently it has been reported that MgO has a good bactericidal performance in aqueous environments and in variety of other industrial applications [5–7]. Consequently, we assessed nanosized nickel oxide which exhibits meticulous properties i.e., catalytic, anomalous electronic and magnetic [5,8,9]. In this paper, we report the bi-metallic of this two oxides (NiO and MgO) as a composite of NiO/MgO for degradation of organic pollutants such as methylene blue (MB) and methylene orange (MO). Large amounts of non-degradable, carcinogenic environmental pollutants such as MB and MO are being discharged by various industries in our streams [10,11]. These dye pollutants are chemically stable, so conventional technologies such as UV radiation and hydrogen peroxide oxidation are not effectively dealing with the problem [10–12]. In this view, prepared NiO/MgO nanocomposite with other metal oxides like TiO_2, ZnO, NiO, MgO and CuO have gained immense research interest as an effective wastewater purification method because of (a) its efficiency in decomposing, (b) mineralising the hazardous organic pollutants as well as the opportunity of utilizing the solar UV and visible spectrum [11,13,14]. Therefore, to the best of our knowledge we report for the first time a simple and environmentally friendly route to synthesis NiO/MgO nanostructures by green approach without using any hash chemicals and reveal their photocatalytic activity.

2. Methods

2.1 Reagents and materials

Skin/peels of pomegranate (Punica granatum L) fruit, were sourced, cleaned and dried in the sun for few days (2–3 days). Metal precursors such as nickel chloride ($NiCl_2$), magnesium chloride ($MgCl_2$), were used in the synthesis and characterisation of the metal oxides while potassium bromide (KBr), potassium hydroxide (KOH) and silver/silver chloride (Ag/AgCl, 3 M) were used in FTIR and electrochemical measurements. 15 mL polyesterine graduated tubes and 0.22 µm hydrophilic filters (Whatman) were used in preparation. Materials and re-agents were purchased from Sigma-Aldrich. The cleanliness of the working electrode was maintained using alumina micropolish (1.0, 0.3, and 0.05 µm alumina slurries) and polishing pads supplied by Buehler, IL, USA.

2.2 Synthesis of green functionalised-NiO/MgO nanostructures

NiO/MgO nanocomposite was prepared according to the method produced by Fuku et al., [15]. Briefly, equimolar amounts of $NiCl_2$ and $MgCl_2$ (10 g — (0.5 mol L^{-1})) were added into a 250 mL round bottle containing yellow peel extract of Punica granatum L or

punicalagin polyphenol (at 80 °C) — which acted as chelating agent and helped form radicals which aided in the formation of NiO/MgO nanostructures. A yellow to dark brown precipitate of NiO/MgO nanostructures, pH 5) was observed. The precipitate was washed (with distilled water) and collected via a combination of sonication (10 min) and centrifugation (10 min, 1000 rpm). Eighty (80%) percent yield of nanopowdered NiO/ MgO was achieved and was dried in an oven at 65 °C, 2 h. After crashing the prepared NiO/MgO nanostructures into a fine powder using mortar and pestle, the nanomaterials were annealed at different temperature (100, 200, 300, 400, 500 and 600 °C) after which they were characterized by different microscopic and spectroscopic techniques.

2.3 Preparation of binary GCE/NiO/MgO nanostructured electrode

Electrochemical measurements of binary NiO/MgO nanostructured glassy carbon electrode (GCE/NiO/MgO) were performed according to earlier reports but with minor adjustments. Briefly GCE electrode was firstly pre-cleaned at +150 mV to −150 mV (20 cycles) using cyclic voltammetry (CV). The electrode was then thoroughly sonicated in both absolute ethanol and deionised water (5 min), respectively, and finally rinsed with distilled water. The cleaned electrode was dried in air (5 min) prior modification. Finally, the nanostructured binary NiO/ MgO was dropcasted (60 μL) onto the GC electrode then dried at 50 °C for 15 min and followed by gently washing with de-ionised water to remove any loosely bound material. Potassium hydroxide solution (2 M, pH 5) was used as the electrolyte for electrochemical measurements.

2.4. Photocatalytic performance evaluation

The scientific community has previously been involved in the photo-degradation of organic pollutants such as methylene blue (MB) and methylene orange (MO) by using metal oxides and their composites. In this paper, we investigated the degradation of MB and MO by using NiO/MgO nanocomposite. Briefly, the effect of NiO/MgO photocatalyst was demonstrated by photo-degradation of MB and MO under ultraviolet light. For convenience MB will serve as an example; MB solution (60 mL) with an initial concentration of 0.6 mg mL^{-1} was transferred into a 20 mL dark brown bottle. Then 10 mg (2 mg mL^{-1}) of NiO/MgO nancomposite (at different temperatures) was also introduced into seven brown bottles. Before irradiation, the aliquots containing MB/MO and catalysts were stirred continuously (30 min) in the dark to reach an adsorption-desorption equilibrium. Further, the system was subjected to UV irradiation which was obtained by 300 W LED light source. The distance between the light source and solution surface was about 5 cm. The sample was irradiate and analysed for the degree of degradation at 10 min successive intervals. After, different concentrations of the catalyst (at 600 ^{o}C) were used to investigate the effect of concentration to the degradation of MB/MO.

3. Instrumentation and apparatus

Particle distribution and morphological studies of NiO/MgO nano-composite was carried out using high-resolution transmission electron microscopy (HR-TEM—Philips Technai-FE 12 TEM instrument operated at an accelerating voltage of 120 kV) and X-ray diffraction (XRD)

performed using a Rigaku D/MAX-PC 2500 X-ray diffractometer. The bi-metallic NiO/MgO nanocomposite composition was enabled using EDS while structural properties and mechanism of the synthesised NiO/MgO nanocomposite were determined by using Fourier transform infrared spectroscopy (FTIR—on a Perkin Elmer spectrometer (Spectrum 100)), and UV–vis measurements were performed using the ocean view fibre optics LED. Finally, a conventional three-electrode connected to autolab instrument (Metrohm) system was used for electrochemical measurements. GC–MS analyses were performed using a GC (Agilent Technologies 7890A) interfaced with a mass-selective detector (MSD, Agilent 7000) equipped with a polar Agilent HP–5 ms (5%-phenyl methyl poly siloxane) capillary column (30m × 0.25 mm i.d. and 0.25 μm film thickness). The carrier gas was helium with the linear velocity of 1 mL/min.

4. Results and discussion

4.1. Formation and crystallinity

To confirm and prove the formation of the nanostructured material is of great importance. The powdered nanocomposite of NiO/MgO was characterized using HRTEM and XRD spectroscopy. These techniques were able to evaluate the particles size, structure, and crystallinity of the NiO/MgO nanocomposite. Fig. 1(a), reveals the formation and crystalline nature of three metal oxides i.e., NiO, MgO, and NiO/MgO nanomaterials at Room temperature (RT). A comparison between the nanomaterials was carried-out in order to differentiate between the metal oxides and finally confirm the formation of NiO/MgO nano-composite. Fig. 1a (i, ii and iii) ascribes the diffraction peaks of pure face-centred cubic NiO NPs with lattice constant (a): 3.52380, pure periclase-MgO NPs with lattice constant (a): 4.21120 and eventually confirmed the formation of face-centred cubic novel binary NiO/MgO nanocomposite with lattice constant (a): 4.19260, respectively.

Fig. 1(b) shows the powdered X-ray diffraction spectrum of grown NiO/MgO nanocomposite at different calcinations temperature. The diffraction structures show crystalline behaviour with 9 peaks. The XRD pattern exhibits prominent peaks at 28.1°, 36.8°, 40.3°, 42.9°, 44.3°, 62.5°, 74.8° and 79.0°.

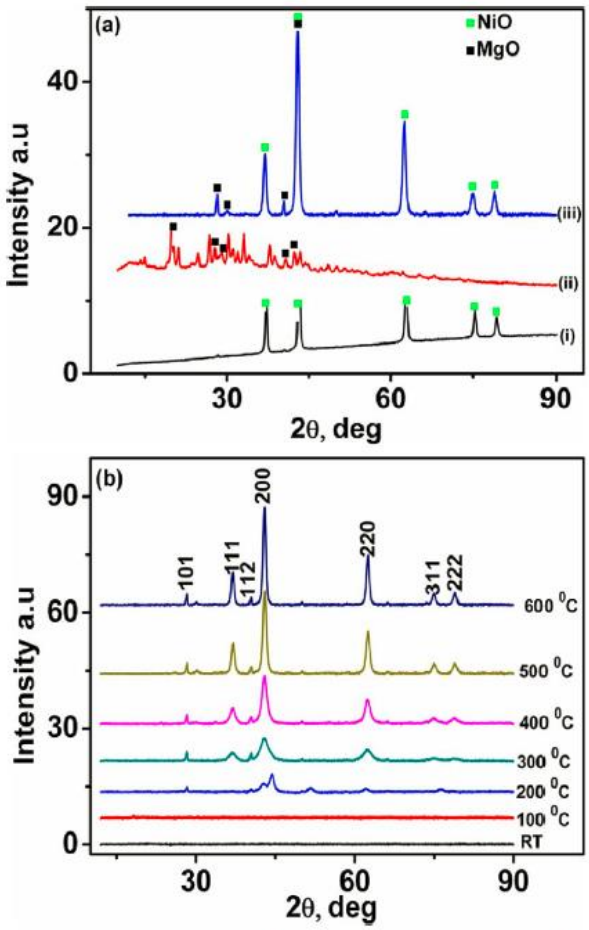

Fig. 1. shows the powdered X-ray diffraction spectrum of grown NiO/MgO nano-composite at different calcinations temperature.

All the reflections were indexed to face-cantered cubic (fcc), and the miller indexes agrees well with the standard data (JCPDS card no. 47–1049 7440-02-0) and literature survey [16–18]. From the diffraction peaks (n = 7) we were able to calculate the crystal size as was observed from our previous studies [15,19]. The mean particle size was calculated to be 3 nm which was found to be in-accordance with the HRTEM results (Fig. 2).The peaks obtained for the nanocomposite are broaden (at low temperatures: RT-400 °C) and becomes more intense as we increase the calcinations temperature (400- 600 °C). The behaviour of the composite indicates that the crystallites are in the nanosized range while showing defects and the intense reflection peaks denotes the growth in the crystallite sizes of NiO/MgO nanocomposite. The crystallinity was concluded through the mean crystallite size as established by TEM particle size and the crystallinity index Eq.(1) [16] is as follows;

$$I_{cry} = \frac{D_p(SEM,\ TEM)}{D_{cry}(XRD)} (I_{cry} \geq 1.00) \qquad (1)$$

where I_{cry} is the crystallinity index; D_p is the particle size (obtained from either TEM or SEM morphological analysis); D_{cry} is the particle size (obtained from the XRD's Scherer

equation). The calculated I_{cry} value ($I_{cry} = 1.6$) of NiO/MgO was found to higher than 1 ($I_{cry} > 1$). The crystalline index result confirmed a polycrystalline NiO/MgO nanocomposite. The obtained index was comparable with chemically and physically prepared binary NiO/MgO nanocomposite. Meanwhile the inter-planar distance was calculated using *Bragg's* Law [16,19] as follows;

$$2dSin\theta = n\lambda \quad (2)$$

where n = 3. λ is the wavelength of the Cu-K_ radiations, θ values corresponding to maximum intensity peak in XRD pattern. The value of λ for the most intense peak was 1.54056 Å. The calculated average interplanar distance (d-spacing) of the synthesised NiO/MgO nanostructures was found to be 0.25 nm.

The size, morphology and particle distribution of the binary NiO/ MgO nanocomposite were also assessed by high resolution-TEM. Fig. 2(a–g) represent the TEM images of the NiO/MgO nanocomposite at different annealed temperatures (RT-600 °C). Upon examination, TEM image of the NiO/MgO nanocomposite, clearly shows amorphous well distributed-uniform spherical nanocomposite with unidirectional lattice fringes and d-spacing ranging from 0.1-0.15 nm (RT–100 °C). However, as we increase the calcination temperatures (200–300 °C), Fig. 2(c-d)) spherical crystalline nanocomposite with multi-directional lattice fringe (d-spacing ranging from 0.15–0.23 nm) and irregular polycrystalline nanostructures become evident (400–600 °C), Fig. 2(e–g). The mean particle size and d-spacing determined by TEM are in reasonable agreement with values calculated from XRD. Conclusively, from both XRD plots and HRTEM images it is apparent that the crystalline nature and the morphological-structures of the prepared nanocomposite depend on higher calcination temperatures. The observed unique behaviour of the nanostructures calls for applications in different fields such as catalysis, energy, biotechnology etc.

4.2. Composition and structure

FTIR and EDS were able to determine the composition of the synthesised nanocomposite. Fig. 3(a) represents the EDS spectrum of the nanocomposite at RT. The EDS spectrum revealed the main components of the NiO/MgO nanocomposite, apparent by very intense Ni (2.4 keV), O (1.4 keV), and Mg (1.4 keV), peaks. The assigned NiO/MgO constituents are in-line with reported [20; 21] energy values. The elemental composition of the prepared nanocomposite provides evidence of the reduced binary metal oxides and is in harmony with the results obtained from XRD. FTIR (Fig. 3 (b)) was also employed to verify the main components and vibrational stretches of the prepared nanocomposite. The spectra (Fig. 3(b)) also provided a possible route of interaction between the reducing ligand (responsible molecule) and the complexes (Ni (II) and Mg (II) ions); thus brought evidence of co-ordination and chelation. Fig. 3(b) also reveal the spectra of control (extract), $NiCl_2$ salt, and $MgCl_2$ salt whilst Fig. 3(c) show the spectra of NiO/MgO nanocomposite at different

annealing temperatures (RT, 100 °C, 200 °C, 300 °C, 400 °C, 500 °C and 600 °C), respectively.

The vibrational stretches of the control/extract are as explained in our previous work [15] whereas those of the metal precursors ($NiCl_2$ and $MgCl_2$), were revealed, Fig. 3(b). Compared to the extract, the IR spectra of the salts (Fig. 3(b)) showed slight shifts (3400, 2000, 1600 and 501 cm^{-1}) in wavenumbers. Furthermore, additional peaks merged at lower regions of the metal salts, 1100 cm^{-1} (not observed on the NiO/MgO) spectra (Fig. 3(c)) and 900 cm^{-1}. The observed peaks were due to the weak ν(O]C]O) and ν(CeO) stretching vibrations. After chelation, a possible mechanism of interaction was proposed (Scheme 1).

The proposed mechanism is as explained in our previous research work [15] with minor adjustments. Briefly; $NiCl_2$ and $MgCl_2$ dissociate into matal ion (Ni^{2+} and Mg^{2+}) when in solution. Thus, Phenolic compounds contained in the extract have hydroxyl and ketonic groups which are able to bind to metals and reduce the metal salt to a nanosize scale. After chelation of the ligands to the metal ions, coordination took place and a complex was formed (Ni^{2+}/Mg^{2+}-polyphenols). Furthermore, to substantiate this coordination and chelation a comparison study of the FTIR spectra between i.e., prepared nanomaterials, metal precursors and the extract was carried out, Fig. 3(b)-(c). Compared to both the metal precursor and the control, the nanocomposite (Fig. 3(c) show a shift and a decrease in wavenumbers at 3450 cm^{-1} (OeH), 1600 cm^{-1} (C = O), and 600 cm^{-1} thus confirming the chelation and coordination of ligands to the metal ions. However, as we vary the annealing temperature (Fig. 3(c)) the deformation of the (OH), ν(C]O) and ν(CeO) vibrational stretch was evident, suggesting deprotonation and formation of the pure NiO/MgO at 468 cm^{-1} region, (Fig. 3(c).

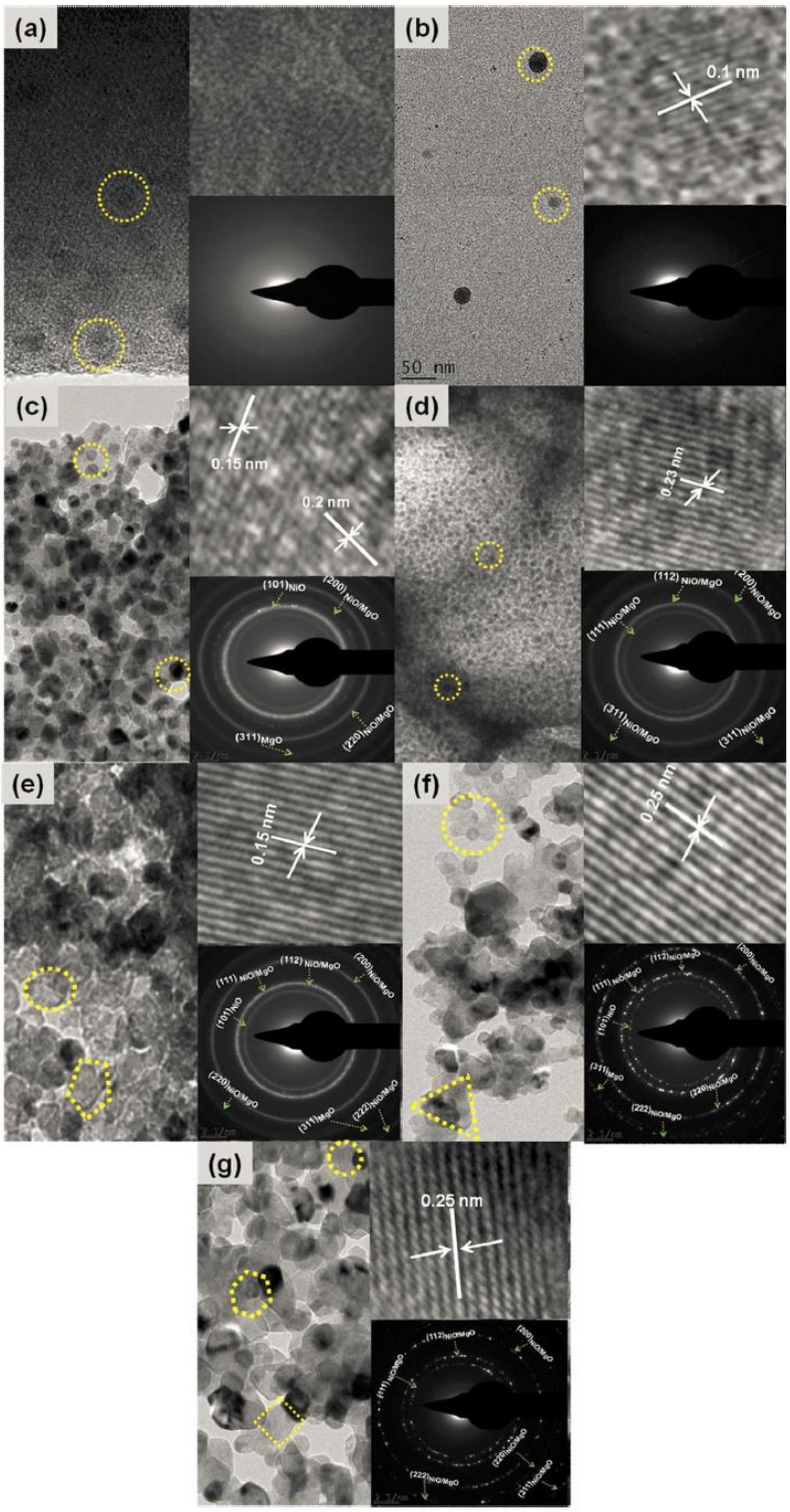

Fig. 2. HRTEM of the prepared NiO/MgO nanocomposite at different annealing temperatures ((a) RT, (b) 100 °C, (c) 200 °C, (d) 300 °C, (e) 400 °C, (f) 500 °C and (g) 600 °C), respectively.

Worth to note, all the impurities at this region (468 cm^{-1}) which are due to the contents of the extracts are removed. The FTIR spectra indicated involvement of the hydroxyl group in the coordination while the metal ions displaced the H^+ and form a complex. The identification of photochemical compounds in pomegranate peel extract by complementary analytical conditions GC/MS analysis was confirmed (Fig. 4), and the decomposition of

the compounds were investigated, Fig. 5(a). Meanwhile, Table 1 represents the main components of the peel extract.

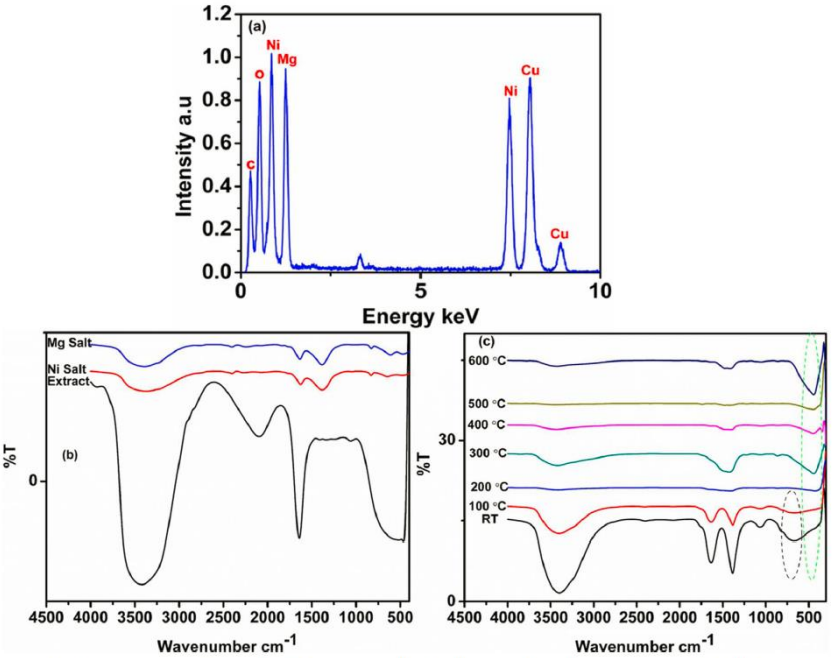

Fig. 3. EDS spectrum of NiO/MgO nanocomposite (a), (b) FTIR spectra of precursor salts and peel extract and (c) FTIR spectra of as-prepared NiO/MgO nanocomposite at different annealing temperatures (RT, 100 °C, 200 °C, 300 °C, 400 °C, 500 °C and 600 °C).

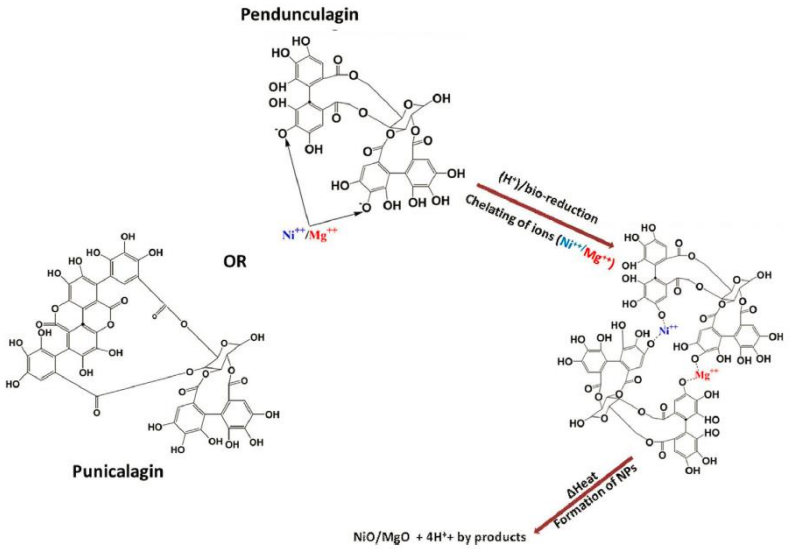

Scheme 1. Schematic representation of the synthetic method/mechanism.

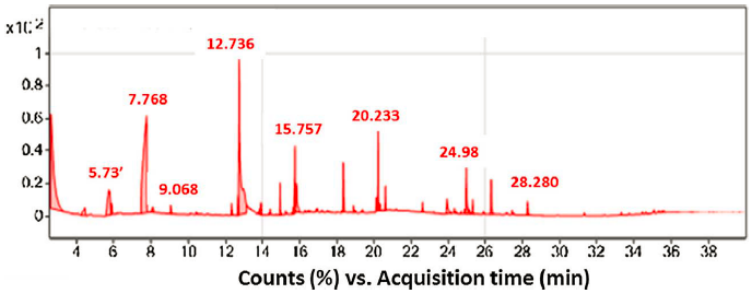

Fig. 4. Chromatogram of methanolic extract of pomegranate peel and.

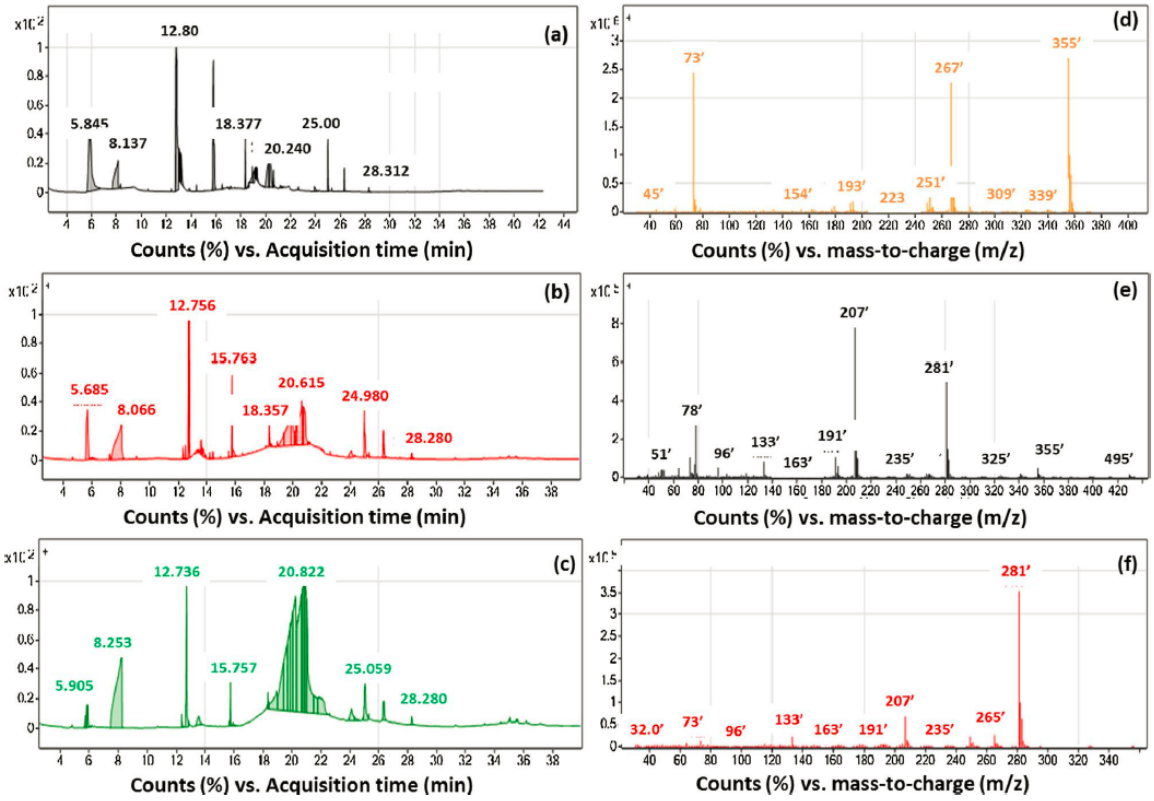

Fig. 5. (A) Chromatograms of pomegranate peel extract at different annealing temperatures (RT, 200 °C and 400 °C).

Table 1
The main components identified by GC–MS in the methanolic extract of pomegranate peel. [25].

Peak no.	RT	% Area	Compounds
1	2.619	80.86	2-Hydroxycyclopent-2-en-1-one
2	7.768	100	Hydroxymethylfurfurole
3	12.736	81.63	Zapotin
4	14.948	4.49	Phenol, 2,4-di-tert-butyl-
5	15.757	12.24	Palmitic acid
6	15.815	10.85	5-formyl −2-furfuryl methanoate
7	18.364	9.66	Cyclohexane,1,2,4,5-tetraethyl cyclohexane
8	20.233	12.66	
9	24.981	10.88	5-methyl-5-octen-1-ol, 9-Octadecanoic acid
10	26.314	6.57	2,6-Pyridinediamine

GC–MS analysis proved presence of different derivatives of major phenols, as shown in Table 1 and the chromatograms are as shown in Fig. 5(a–c). As shown in Table 1, some identified phenolic compounds are present from peel extract as observed at Rts (2.619, 7.768, 12.736, 14.948, 15.757, 15.815, 18.364, 20.233, 24.981, 26.314 min) with a high percentage as (80.86%, 100%, 81.63%, 4.49%, 12.24%, 10.85%, 9.66%, 12.66%, 10.88%, 6.57%), respectively. The chromatograms of these compounds are as presented in Fig. 5. The phenolic compounds of the pomegranate peel extract contain phenolics, flavonoids, ellagitannins (ETs), and proanthocyanidin compounds. The derivatives of major compounds as Punicalagin, one of ellagitannins (ETs), then produce derivatives, as a glycone –sugars moiety of glycoside as DL- Xylose and 1-Deoxy-D-arabitol, respectively.

The spectra and compounds are in line with those reported by others [25]. The spectra confirm that there were many constituents found at RT compared to other annealing temperatures. At RT (Fig. 5(a and d)) phenolic compounds were in abundance providing evidence of the extracted reducing agents. Nonetheless, as we move to higher temperatures 200 °C (Fig. 5(b–f)) the polyphenols decompose and eventually leaves only the responsible reducing compounds i.e., punicalagin and penduculagin. The obtained results are in accord with the FTIR data and confirm the mechanism of interaction as provided. However, at optimal temperature of 200 °C – 400 °C (Fig. 5(a–f)) the molecules were distinguished by their characteristic fragment ion spectra yielding sequential losses of Hydroxymethylfurfurole (m/z 32), Zapotin (m/z 64), 2-Hydroxycyclopent-2-en-1-one (m/z 119), Phenol, 2,4-di-tert-butyl (m/z 133), Palmitic acid (m/z 177), 5-formyl –2-furfuryl methanoate (m/z 191), and Cyclohexane,1,2,4,5-tetraethyl cyclohexane (m/z 193). Isomers 8 and 9 yielded two ions at m/z 210 and 280, corresponding to singly and doubly-charged punicalagin isomer ions, respectively. The single charge m/z 210 ion was detected in both experimental conditions and was characteristic of punicalagins, the main ellagitannins described in pomegranate peels. The doubly charged ion, was mainly detected and gave fragments at m/z 240, 265, and 601 a fragmentation pattern also consistent with punicalagin.

4.3. Optical and electrochemical properties

UV-vis was employed to investigate the wavelength maxima (λ_{max}), band gap energies and the effect of temperature (RT, 100 °C, 200 °C, 300 °C, 400 °C, 500 °C and 600 °C) on the synthesised NiO/MgO nanocomposite, Fig. 6. Two distinctive absorption peaks at λ_{max} = 292 nm and 354 nm were observed. The λ_{max} at 354 nm was due to the presence of NiO nanoparticles while that of MgO was visible at 296 nm (Fig. 6(a)). However, a new absorption peak was noted at λ_{max} = 452 nm and was associated with the formation of NiO/MgO nanocomposite. Further, the spectra also confirm the formation of NiO/ MgO nanocomposite due to the presence of both NiO and MgO nanoparticles. The results are in agreement with both XRD and HRTEM data.

The bandgap energies (Planck's equation) [15] calculated from different λ_{max} were found to be $E_g(NiO)$ = 3.50 eV, $E_g(MgO)$ = 4.11 eV and $E_g(NiO/MgO)$ = 2.74 eV. Meanwhile, the NiO/MgO nanocomposite appeared to be highly conductive compared to the NiO and MgO

nanoparticles. Fig. 4 was also used to distinguish between the effects of temperature on the as-prepared nanocomposite. Compared to NiO/ MgO at RT, the nanocomposite at different temperatures showed a decrease and a shift in λ_{max} suggesting a change in particle size and band gap energies. A broader absorption peak at 452 nm was observed (room temperature (RT)) which decreases in intensity as we increasing the temperature (100 °C – 600 °C). There was also a shift in the wave maxima due to quantum confinement and a change in particle size.

The redox properties, electrochemical properties and formation of NiO NPs, MgO NPs and NiO/MgO nanocomposite were investigated with the help of cyclic voltammetry (CVs). The electrochemical characteristics were carried out in 0.1 M KOH over the wide range of voltage −1.5 V to +1.5 V (vs. Ag/AgCl) at 0.1 V/s. Typical CVs of GCE/ NiO (at 200 °C), GCE/MgO (at 200 °C) and GCE/NiO/MgO (at 200 °C and 600 °C) are shown in Fig. 7.

Fig. 7(a) and (b) reveals quartz-reversible couples (oxidation ($E_{p,a}$) – reduction peaks ($E_{p,c}$)) due to both NiO NPs and MgO NPs, respectively. The couples were found at $E_{p,a}$ = 550 mV (Fig. 7(a) a) and $E_{p,c}$ = − 450 mV (Fig. 7(a) b) and those of NiO NPs were observed at $E_{p,a}$ = 700 mV (Fig. 7(b) a), $E_{p,c}$ = 480 mV (Fig. 7(b) c), $E_{p,a}$ = 120 mV (Fig. 7(b) b –irreversible) and $E_{p,c}$ = − 420 mV (Fig. 7(b) d)-irreversible). The peak potentials confirmed the electrochemical properties of the NPs and are in agreement with other published work. Fig. 7(c) shows the formation, shift and properties of the prepared NiO/MgO nanocomposite. Fig. 7(c) a and e, shows the MgO couples while those of NiO were shown in Fig. 5(c) b,c,d and e which are present in the voltamogram of NiO/MgO nanocomposite, Fig. 7. On the other hand, Fig. 7(d) examines the behaviour of two electrodes (GCE/NiO/MgO) at 200 °C and 600 °C. Compared to GCE/NiO/MgO) at 600 °C, GCE/NiO/MgO) at 200 °C revealed redox couples (see figure (c) labelling) of which some are not present in the latter (Fig. 7(a) a and e). The results confirmed that the nanocomposite are temperature dependent and are in agreement with other techniques i.e., TEM, UV–vis and FTIR.

From Fig. 7, we were able to calculate the band gap energy of the synthesised nanocomposite from all the redox couples by using an equation reported by Fuku et al. [15]. The band gap energies of the asgrown NiO/MgO nanocomposite at 200 °C and 600 °C annealing temperature were calculated to be E_g = 3.8 eV (200 °C) –and 2.9 eV (600 °C), respectively. The electrochemical band gap energies are comparable with the measured optical energies. In their paper, Jun et al., [22], synthesised NiO/MgO nanocomposite using a plant extract and their calculated band gap energies were in agreement with our results.

4.4. Photocatalysis

In the present study, methylene orange (MO) and methylene blue (MB) were employed as a target pollutants to evaluate the real performance of the as-prepared catalyst (NiO/MgO) under visible-light illumination. Photocatalytic degradation of MO and MB were studied using UV–vis and scanned in the range of 190–800 nm, before and after ultra-violet light

interaction (Fig. 8). Fig. 8(a) present the maximum absorption plots of MB and MO before exposure, mixture of both MO + NiO/MgO (before and after exposure) and MB + NiO/MgO (before and after exposure). The absorption λ_{max} of NiO/MgO nanocomposite was at 452 nm whilst MO had two characteristic absorbance peaks at λ_{max} = 270 nm and λ_{max} = 466 nm and the mixture of MO + NiO/ MgO with ratios 1:2 showed the same λ_{max} as MO but with slightly decrease in absorbance intensities. Meanwhile, the absorption maxima of MB was at λ_{max} = 290 nm and λ_{max} = 630 nm while the mixture of MB + NiO/MgO had a λ_{max} = 646 nm. Fig. 8(a) shows the effect of illumination time at selected λ_{max} (MO = 466 nm and MB = 646 nm), respectively. The degradation of MO and MB without the catalyst under UV illumination showed a slight/no change in the absorbance intensities confirming the need of a catalyst and it attests that photo-catalytic degradation is a feasible means of organic pollutants removal from wastewaters. After mixing the pollutants (MO and MB) with the catalyst (NiO/MgO), a slight decrease in absorption intensity was observed before irradiation. This was attributed to the good crystallinity, wide visible-light absorption range, and the efficient electron-hole pair separation properties of the NiO/MgO nanostructures [10]. The behaviour suggests or confirms the formation and adsorption of the materials (catalyst + pollutant). After 2 min of exposure the catalyst degraded the pollutant by 34%, suggesting a good catalytic effect of the nanocomposite. However, after 10 (MO) and 12 (MB) min saturation of the pollutants was observed, respectively. Thus, the optimum illumination time for degradation of MO and MB was noted as 10 and 12 min. Many compounds were decomposed entirely after 3–5 h [11,23,24]. Therefore, the results suggest that the catalyst was efficient for the decomposition of MO and MB. The nanocomposite showed better interaction and decomposition of the pollutants compared to other findings [10,24].

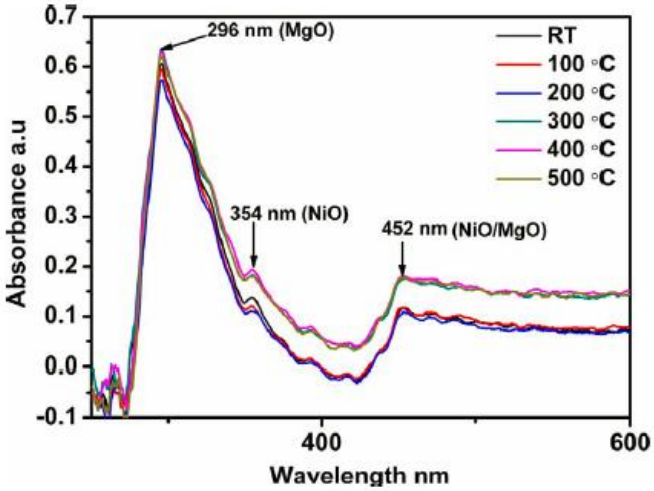

Fig. 6. UV–vis spectra of as-prepared NiO/MgO nanocomposite at different annealing temperatures (RT, 100 °C, 200 °C, 300 °C, 400 °C, 500 °C and 600 °C).

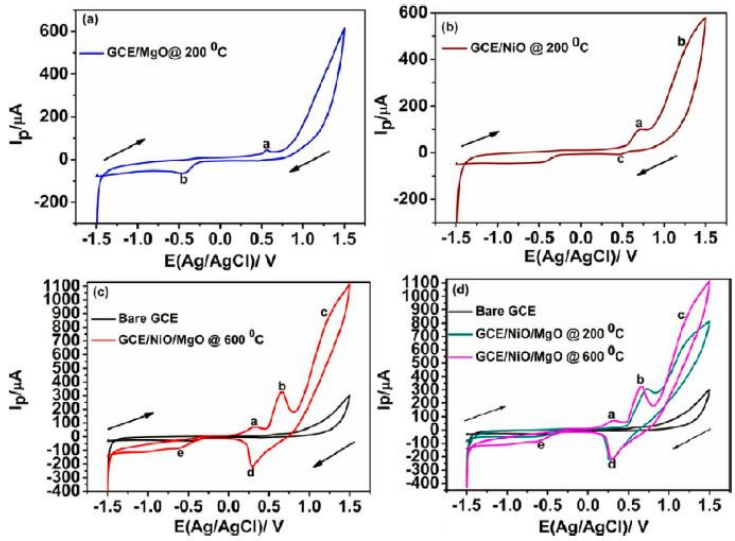

Fig. 7. CV spectrum/specta of as-prepared (a) GCE/MgO NPs at 200 °C (b)GCE/NiO NPs at 200 °C, (c) GCE/NiO/MgO nanocomposite at 600 °C and (d) GCE/NiO/MgO nanocomposite at 600 °C.

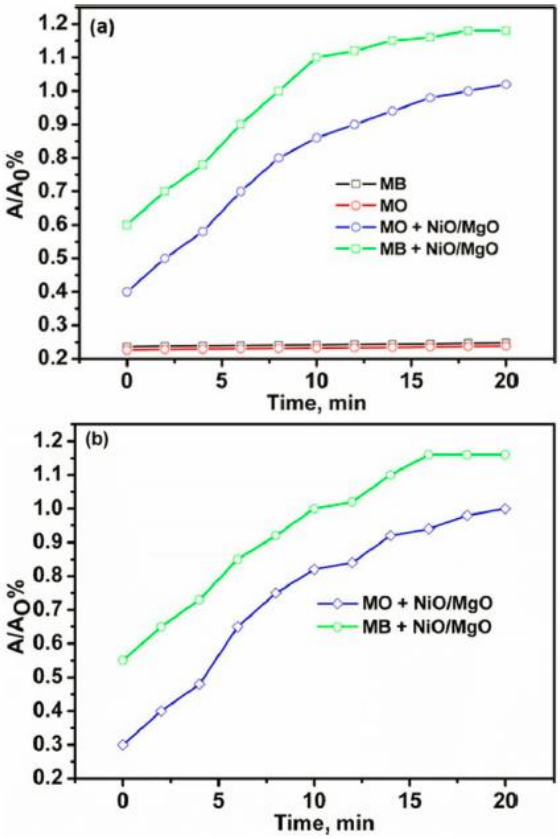

Fig. 8. UV–vis spectra of (a) MB and MO in the presence and absence of NiO/MgO nanocomposite at different UV-exposure time and (b) the reusability curve of the catalyst.

The percent degradation of MO and MB were calculated as follows;

$$\%D = \frac{(A_0 - A_t)}{A_0} \times 100 \qquad (3)$$

where D is the percent degradation, A_O is the absorbance of initial MO; A_t is the absorbance of the solution after illumination. The catalyst degraded the pollutants by 73 — 87% at 2 mg mL^{-1} concentration of NiO/MgO, 0.6 mg mL^{-1} concentration of pollutants at 10 min illumination time, Fig. 8(a). The behaviour proves the excellent photocatalytic activity of the as-prepared sample under visible light irradiation. The test demonstrates that no dye degradation in solution can be observed in the absence of the photocatalyst at the same conditions from a blank experiment. NiO/MgO material showed improved separation of photo-induced electron-hole pairs owing to the potential-energy, therefore NiO/MgO exhibited enhanced photocatalytic activity. Table 2 below confirms the superiority of the prepared NiO/MgO nanocatalyst.

Reusability and stability is an important tool of heterogeneous catalyst for industrial application. Therefore, the stability and reusability of NiO/MgO nanocomposite was carried out as shown in Fig. 8(b). The reusability of *NiO/MgO* was tested by centrifuging the nanocatalyst from the dye solutions, after which it was washed (distilled water) and dried at 100 °C in an oven. Further, the stability of *NiO/MgO* nanocomposite was evaluated under the same condition as the freshly prepared nanocomposites. The photostability of the *NiO/ MgO* photocatalyst was carried out by recycling the experiment for the degradation of MB and MO. The reused catalyst showed a similar response to that of the fresh catalyst, highlighting the stability and reusability of *NiO/MgO nanocomposite*. The schematic band structure and charge transfer process of the NiO/MgO nanocatalyst is presented in Fig. 9.

Table 2
Comparison of photocatalytic activity of different nanocatalysts using the same organic pollutant.

Catalyst used	Catalyst preparation method	Organic pollutant	Degradation efficiency (%)	Irradiation time (min)	Reference
NiO/MgO	Green biosynthesis	MB MO	73–87	10	[19]
rGO/ TiO2/ ZnO	Solvothermal	MB MO	92 47–68	120	[15]
Fe3O4/ CuO/ ZnO/ NGP	Sol-gel	MB	57–87	120	[16]
Fe-doped CeO2	Homogeneous/ impreganation	MO	–	120	[18]
ZnO/CuO	Hydrothermal	MB	99	15–25	[21]
CuO	Green biosynthesis	MB MO			[22]
ZnFe2O4	Discharge	MB	84	300	[20,22]
ZnFe2O4/ MWC-NT			99		

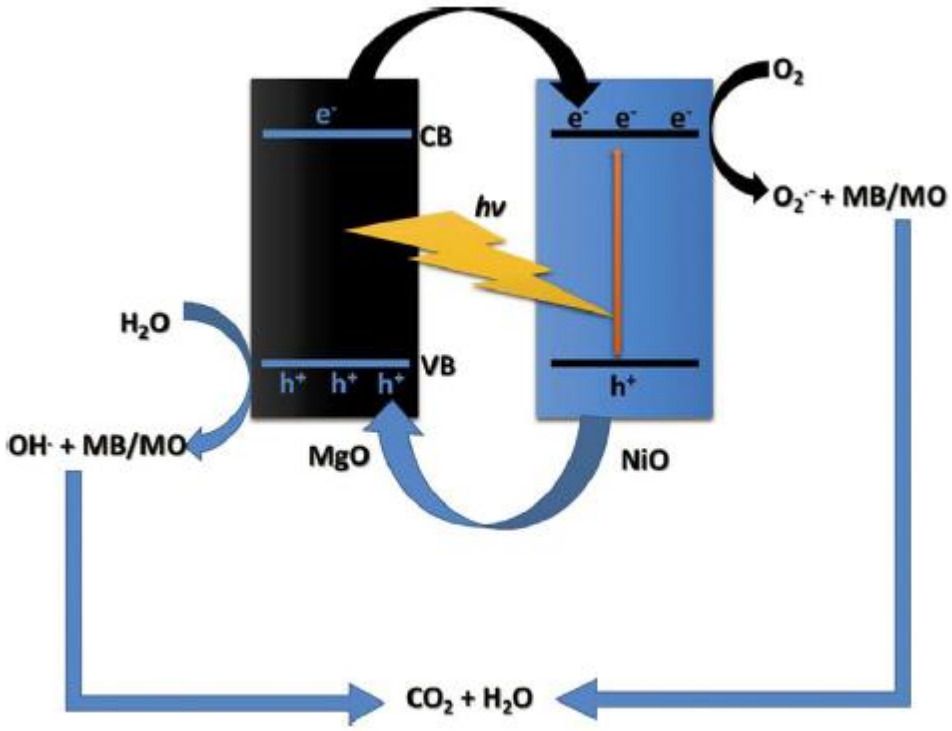

Fig. 9. Mechanism of photocatalytic degradation.

The photo-induced electron–hole pairs are separated from each other in NiO under UV irradiation. The electrons transit from the valence band (VB) to the conduction band (CB) and leave positive holes (h^+) in VB. After separation of electrons and holes, the dissolved oxygen (O_2) adsorbed on NiO surface will react with photo-induced electrons to form superoxide radical ($\cdot O_2^-$). Considering the band structures of ZnO and CuO, direct transfer of photo-induced holes from MgO to NiO thermodynamically occurs in the NiO/MgO nanocatalyst, leading to low recombination rate of the photo-induced electronhole pairs. The hydroxyl ions (-OH) will be oxidized into hydroxyl radicals (·OH) by photo-induced holes [26]. Finally, the dye molecules are decomposed into simple organics by the continuous generated reactive oxidation species and further converted into CO_2 and H_2O. Therefore, the enhanced photocatalytic degradation of the NiO/MgO nanocatalyst should be attributed to the effective charge-transfer between NiO and MgO.

5. Conclusion

Nanostructured composites of NiO/MgO have been synthesized through bio-reduction method using nickel chloride, magnesium chloride and peel extracts of punica granatum L. The use of punica granatum L extract as reducing agents for the formation of bimetallic metal oxides (NiO/MgO nanocomposite) served as an innovative idea in this work. The simplicity and the green-modification in the method make it eco-friendly in nature while becoming useful in several applications i.e., water pollution and related application. XRD and HRTEM confirmed the formation of highly crystalline face-centred cubic novel binary NiO/MgO nanocomposite with lattice constant (a): 4.19260. Conclusively, from both XRD plots and HRTEM images it is apparent that the crystalline nature and the morphological-structures of the prepared nanocomposite depend on higher calcination temperatures. The observed unique behaviour of the nanostructures calls for applications in different fields such as catalysis, energy, biotechnology and others. However, the nanocomposite gave good response in photo-catalysis applications. UV–vis and CV characterisations studies were also carried out with the aim finding the λ_{max} and conductivity of the materials. Energy band gaps at different λ_{max} were found to range from 1.2–3.83 eV suggesting a very conductive semiconductor. FTIR and EDS confirmed the mechanism of interaction. In the present study the water extract of the peels of two species of punicalagin and penduculagin were subjected to GC–MS analysis. Twenty-one and 14 compounds were identified in punicalagin and penduculagin extracts, respectively. The as-prepared NiO/MgO nanocomposite proved to be a significant catalyst for photocatalytic degradation of MB and MO. The experiment revealed that the presence of NiO/MgO nanocomposite was necessary for the degradation of pollutants at 5–10 mg mL^{-1} (concentration of catalyst) with short illumination time of 10 min. The research indicates that NiO/MgO catalyst is a potential candidate for photo-oxidation of organic dye in industrial wastewater. In addition, its proven that the nanocomposite have good photocatalytic stability in the degradation of MB under UV light irradiation after the recycling process. Conclusively, the green synthesised NiO/MgO nanocomposite may be suitably used as a new catalytic agent for wastewater treatment, pharmaceutical and biomedical applications.

Conflict of interest
The authors declare that they have no competing interests.

Acknowledgements
The authors would like to thank iThemba Labs and NRF for the financial support. We acknowledge Department of Materials Division (MRD) and the University of the Western Cape for providing us with state-of-the-art instruments and Labs.

References

[1] H. Chang, C. Lo, L.C. Chen, T.T. Tsung, C.S. Jwo, Photodecomposition and surface adsorption of methylene blue on TiO_2 nanofluid prepared by ASNSS, Materi. Trans. 45 (2004) 3334–3337.

[2] S. Rehman, Size effects on the magnetic and optical properties of CuO nanoparticles, J. Nanopart. Res. 13 (2011) 2497–2507.

[3] E. Christian, Selective synthesis of clinoatacamite $Cu_2(OH)_3Cl$ and tenorite CuO nanoparticles by pH control, J. Nanopart. Res. 16 (2014) 25–56.

[4] A. El-Trass, CuO nanoparticles: synthesis, characterization, optical properties and interaction with amino acids, Appl. Surf. Sci. 258 (2012) 2997–3001.

[5] C. Mahendirana, K. Scottb, A. Gedankena, Synthesis of a carbon-coated NiO/MgO core/ shell nanocomposite as a Pd electro-catalyst support for ethanol oxidation, Mater. Chem. Phys. 128 (2011) 341–347.

[6] Y. Kawaguchi, Luminescence spectra at bending fracture of single crystal MgO, Solid State Commun. 117 (2000) 17–20.

[7] K. Kaviyarasu, A versatile route to synthesize MgO nanocrystals by combustion technique, Der Pharma Chem. 3 (2011) 248–254.

[8] A.S. Danial, S.A. Salih, M.I. Awad, On the synthesis of nickel oxide nanoparticles by sol–gel technique and its electrocatalytic oxidation of glucose, J. Power Sources 293 (2015) 101–108.

[9] M. El-Kemary, I. El-Mehasseb, Nickel oxide nanoparticles: synthesis and spectral studies of interactions with glucose, Mater. Sci. Semicond. Process. 16 (2013) 1747–1752.

[10] D. Zhang, Synergetic effects of Cu_2O photocatalyst with titania and enhanced photo-activity under visible irradiation, Acta Chim. Slovaca 6 (2013) 141–149.

[11] W. Wang, S. Yang, Photocatalytic degradation of organic dye methyl orange with phosphotungstic acid, J. Water Resour. Prot. 2 (2010) 979–983.

[12] D. Briggs, Environmental pollution and the global burden of disease, Br. Med. Bull. 68 (2003) 1–24.

[13] H. Siddiqui, F.Z. Haque, Structural and optical properties of cuo nanocubes prepared through simple hydrothermal route, Int. J. Sci. Eng. Res. 5 (2014) 2229–5518.

[14] R. Sathyamoorthy, K. Mageshwari, Synthesis of hierarchical CuO microspheres: photo-catalytic and antibacterial activities, Phys. E 47 (2013) 157–161.

[15] X. Fuku, N. Matinise, M. Maaza, Punicalagin green functionalized $Cu/Cu_2O/ZnO/CuO$ nanocomposite for potential electrochemical transducer and catalyst, Nanoscale Res. Lett. 11 (2016) 356.

[16] N. Rifaya, M. Alagar, Chemical capping synthesis of nickel oxide nanoparticles and their characterizations studies, Nanosci. Nanotechnol. 2 (2012) 134–138.

[17] J. Suresh, A.J. Nathanael, M. Sundrarajan, S.I. Hong, Antibacterial and wash durability properties of untreated and treated cotton fabric using MgO and NiO nanoparticles, Appl. Mech. Mater. 508 (2014) 48–51.

[18] K.G. Chandrappa, B.M. Praveen, B.S. Shylesha, Generation of nanostructured MgO particles by solution phase method, Res. J. Chem. Sci. 5 (2015) 13–18.

[19] T. Theivasanthi, An insight analysis of nano sized powder of jackfruit seed, Nano Biomed.
Eng. 3 (2011) 163–168.
[20] Y. Li, Y. Wang, catalyst prepared via dielectric-barrier discharge plasma with improved catalytic performance for carbon dioxide reforming of methane, Front. Chem. Sci. Eng. 8 (2014) 133–140.
[21] A. Faris, A. Islam, Z. Zainal, High coke-Resistance Pt/Mg1-xNixO catalyst for dry reforming of methane, PLoS One 1 (2016), http://dx.doi.org/10.1371/journal.pone. 0145862.
[22] J. Wang, Z. Li, X. Jing, Z. Jiang, Synthesis of chrysalis-like CuO nanocrystals and their catalytic activity in the thermal decomposition of ammonium perchlorate, J. Chem. Sci. 121 (2009) 1077–1081.
[23] D. Singh, Synthesis of copper oxide nanoparticles by a novel method and its application in the degradation of methyl orange, Adv. Electron. Electr. Eng. 1 (2014) 83–88.
[24] X.T. Zhou, X.J. Huang, Photocatalytic degradation of methyl orange over metalloporphyrins supported on TiO_2 degussa P25, Molecules 17 (2012) 1149–1158.
[25] P. Mena, G. Galaverna, Rapid and comprehensive evaluation of (poly) phenolic compounds egranate (punica granatum l.) juice by UHPLC-MSN, Molecules 17 (2012) 14821